Structure–Morphology and Tear Strength of Oriented Tapes of Polyethylene and Its Blends. III

S. J. MAHAJAN,[1] B. L. DEOPURA,[1,*] and YIMIN WANG[2]

[1]Textile Technology Department, Indian Institute of Technology, New Delhi 110016, India, and [2]Chemical Fibre Research Institute, China Textile University, Shanghai 200051, China

SYNOPSIS

The tear energy (G_c) of high-density polyethylene (HDPE) and HDPE/ethylene copolymer blended drawn tapes in orientation direction has been studied systematically with respect to structural parameters. In all cases the values of G_c were in the range of 0.8–8.0 kJ m^{-2}. The results showed a direct relationship between amorphous phase orientation and G_c of drawn tapes. The decrease in G_c with molecular orientation of tapes is due to the formation of large number of elongated voids at the interfibrillar regions and diminution of viscous flow occuring in the vicinity of the propagating crack tip. An increase in G_c in the range of 15–45% was obtained for HDPE blended tapes containing about 10% of the second-blend component either as ethylene-vinyl acetate or ethylene propylene-diene terpolymer or ethylene-propylene block copolymer. This relates to the increase in fraction of amorphous phase and extensive molecular network in the interfibrillar amorphous regions.

INTRODUCTION

Fracture surface energy (G_c) of conventionally oriented semicrystalline polymers in a tearing mode has been studied previously.[1-11] However, there are only few reports on structural investigations and the effect of structure on tearing behavior of polyethylenes[2,5,6,8-11] and on polyolefin blends.[10,11] Some of the earliest attempts to measure fracture surface energy of thin thermoplastic polymeric films were made by Anderton and Treloar[2] for various polyethylenes and by Sims[3] for isotactic polypropylene (PP), using the tear test originally developed by Rivlin and Thomas.[4] Anderton and Treloar[2] determined G_c for three different grades of low-density polyethylene (LDPE), and one grade of high-density polyethylene (HDPE). They found that G_c of undrawn LDPE and HDPE films was of the order of 160 and 80 kJ m^{-2}, respectively. They further noted that G_c dropped by a factor of about 100 when uniaxially oriented films were used and related the decrease in G_c to the formation of sharper crack tip and reduced tendency of drawn films to undergo plastic deformation near the crack tip. Similar results have also been reported by Clements and Ward.[5]

In this article studies on tearing behavior of HDPE/ethylene copolymer blended tapes in orientation direction are presented. The effects of fraction of amorphous phase and its orientation and of void dimensions on tearing behavior are examined.

EXPERIMENTAL

Materials

HDPE, LDPE, PP, high-molecular-weight high-density polyethylene (HMWPE), linear low-density polyethylene (LLDPE), ethylene-vinylacetate (EVA), ethylene-propylene-diene terpolymer (EPDM), and ethylene–propylene block copolymers (EP_bC) were used in the present work. The melt flow index (MFI) density and other relevant information of these materials are given in Table I.

* To whom the correspondence should be addressed.

Journal of Applied Polymer Science, Vol. 60, 1539–1549 (1996)
 CCC 0021-8995/96/101539-11

Table I Characteristics of Materials Used

Polymer Type	Commercial Code	Supplier	MFI*	Density (g/cm^3)	Comonomer Type and Composition
HDPE	GF 7745F	PIL, India	0.7	0.945	1.8 CH_3/100 C
HMWPE	GF 7755	PIL, India	0.4	0.953	2.1 CH_3/100 C
LLDPE	Dowlex-2045E	Dow Chem. USA	1.0	0.920	3.2 CH_3/100 C (L-octene)
LDPE	Dowlex-200	Dow Chem. USA	0.9	0.920	3.6 CH_3/100 C
EVA	Elvax-4210	DuPont, USA	0.8	0.928	4.7 mol % vinylacetate
EPDM	Nordel-1040	DuPont, USA	40+	0.560	75 mol % ethylene and 4 mol % diene
PP	S-3030	IPCL, India	3.0	0.910	Isotactic homopolymer
EP_bC 1.5	MI-1530	IPCL, India	1.5	0.900	6.9 mol % ethylene
EP_bC 3.5	MI-3530	IPCL, India	3.5	0.900	6.8 mol % ethylene
EP_bC 7.0	MI-7040	IPCL, India	7.0	0.900	7.2 mol % ethylene
EP_bC 13.0	MI-0030	IPCL, India	13.0	0.900	6.6 mol % ethylene

* ASTM D1238/L.
† Moony viscosity 40, measured at ML4 at 121°C.

Sample Preparation

Uniaxially drawn tapes of HDPE/ethylene copolymer blends, HDPE/PP and HDPE/EP_bC blends were prepared using a Betol-1820, single screw extruder of L/D ratio 20, screw dia of 18 mm, and a bottom-fed slit die having width and thickness dimensions of 13 and 0.4 mm, respectively. The temperature profile used for extrusion was 160°C at the feed zone, 200°C at the compression zone, and 220°C at the metering zone and the die end. The screw speed was kept at 12 rpm. The as-extruded tapes were immediately quenched in a water bath maintained at 30°C and were drawn in sequence on a 750-mm-long hot plate maintained at 95°C with a draw ratio of 10×. The drawn tapes were collected on a take-up bobbin with a speed of about 10 m/min. The drawn tapes were in the range of 950–1000 denier (denier is the weight in grams of 9000 meters of tape). The weight percent composition of blend components used for preparation of various blended tapes are summarized in Table II.

To study the effect of molecular orientation on fracture surface energy, HDPE tapes with draw ratios of 3×, 5×, 7×, and 14× were also prepared.

Characterization of Oriented Tapes

Wide-Angle X-ray Diffraction

The drawn tapes were characterized for crystallite and amorphous phase orientation using wide-angle X-ray diffraction (WAXD) and polarizing microscopy. The details of these characterization techniques, methods of analysis, and the results has been described elsewhere.[12,13] The results of few selected specimens are given in Table III.

Small-Angle X-ray Scattering

The small-angle X-ray scattering (SAXS) measurements were carried out on a slit collimated diffractometer of Rigaku–Denki, with CuK_α radiation. For equatorial measurements, uniaxially oriented thin tapes were aligned accurately with the tape axes parallel to the slit, whereas for meridional measurements, tapes were placed next to each other over a length of X-ray beam (tape axes perpendicular to the slit) by mounting the thin tapes on a rectangular sample holder. The absolute values of the scattered intensity was obtained by means of filter attenuation. The mean void dimensions in equatorial and meridional directions were estimated from the slope of Lorentz factor corrected Guinier plots [$\ln(s)$ vs. (s^2)].[14–17]

Table II Blend Composition for Various Blend Systems

Polymer Blend System	Blend Components	Blend Composition (wt %)
HDPE/ethylene copolymer blends	HDPE/HMWPE	90/10
	HDPE/LLDPE	90/10
	HDPE/LDPE	90/10
	HDPE/EVA	90/10
	HDPE/EPDM	90/10
HDPE/PP and HDPE/EP_bC blends	HDPE/PP or EP_bC	91/9
		82/18
		50/50
		20/80
		0/100

Table III Structural Characteristics of HDPE Blended Tapes*

Sample	$(1 - X_c)$	$f_{am(avg)}$	G_c (kJ m^{-2})	l_e (Å)	l_m (Å)	$\phi_v \times 10^4$ (cm^3/cm^3)	$N_v \times 10^{-14}$ (cm^{-3})
HDPE (control)	0.26	0.50	0.86	122	144	15.6	13.9
10 HMWPE	0.29	0.57	0.88	—	—	—	—
10 LLDPE	0.32	0.48	0.91	150	160	14.9	7.9
10 LDPE	0.33	0.43	1.02	163	169	21.5	9.2
10 EVA	0.40	0.39	1.17	151	156	17.1	9.2
10 EPDM	0.35	0.31	1.25	173	164	13.4	5.5
9 PP	0.30	0.50	0.90	158	173	18.3	8.1
18 PP	0.30	0.55	0.92	—	—	24.0	—
50 PP	0.41	0.30	0.80	169	190	25.8	9.1
80 PP	0.42	0.31	0.80	—	—	27.9	—
100 PP	0.35	0.44	0.84	154	161	22.2	11.2
9 EP$_b$C	0.39	0.49	1.12	148	159	15.0	8.2
18 EP$_b$C 1.5	0.30	0.51	0.98	—	—	16.1	—
50 EP$_b$C 1.5	0.43	0.47	0.84	—	—	14.5	—
80 EP$_b$C 1.5	0.44	—	0.91	—	—	19.3	—
100 EP$_b$C 1.5	0.45	0.42	1.10	—	—	14.3	—
9 EP$_b$C 3.5	0.39	0.53	1.00	163	172	18.9	7.9
18 EP$_b$C 3.5	0.37	0.53	0.78	—	—	19.8	—
50 EP$_b$C 3.5	0.41	0.32	0.79	174	191	28.7	9.5
80 EP$_b$C 3.5	0.41	0.34	0.82	—	—	30.2	—
100 EP$_b$C 3.5	0.44	0.42	1.05	160	178	23.6	9.9
9 EP$_b$C 7.0	0.31	0.37	1.02	—	—	19.8	—
50 EP$_b$C 7.0	0.54	0.34	0.75	—	—	36.1	—
9 EP$_b$C 13.0	0.25	0.41	0.96	165	188	21.9	8.2
18 EP$_b$C 13.0	0.23	0.53	0.87	—	—	35.5	—
50 EP$_b$C 13.0	0.41	0.36	0.72	—	—	—	—
80 EP$_b$C 13.0	0.42	0.36	0.74	—	—	47.0	—
100 EP$_b$C 13.0	0.43	0.48	0.98	152	171	30.5	14.7

* Draw ratio 10X; drawing temperature 95°C.

Density

The density of drawn tapes was obtained using Davenport density gradient column.[12] A liquid mixture of isopropyl alcohol and di-ethylene glycol was used for this purpose.

DSC Crystallinity

A Perkin–Elmer, differential scanning calorimeter (DSC) was used to measure the heat of fusion of drawn tapes. The total weight fraction crystallinity $[X_{c(dsc)}]$ was determined using the heat of fusion of 100% crystalline PE and PP as 293 and 163 J/g, respectively.[18]

Volume Fraction of Voids and Void Number Density

The volume fraction of voids (ϕ_v) of drawn tapes was estimated by the combination of DSC crystallinity and density values according to the relationship proposed by Bodaghi et al.,[19] which can be expressed as

$$\phi_v = 1 - \frac{\rho_s[X_{c(dsc)}]}{\rho_c} - \frac{\rho_s[1 - X_{c(dsc)}]}{\rho_{am}} \quad (1)$$

where ϕ_v is the total volume fraction of voids in the drawn tapes, ρ_s is the measured tape density, ρ_c is the intrinsic crystalline phase density, ρ_{am} is the intrinsic amorphous phase density, and $X_{c(dsc)}$ is the total weight fraction of crystalline material determined by DSC technique. The void number density per unit volume (N_v) is computed from the total volume fraction of voids and the average volume of a void determined from mean void dimensions in meridional and equatorial directions, assuming that the voids are of elliptical shape.

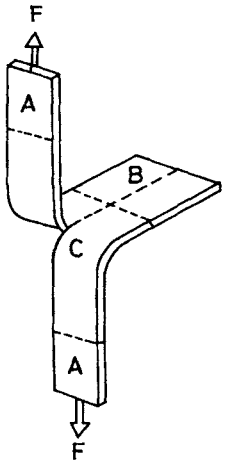

Figure 1 Tear-test specimen showing strain distribution: uniform strain region (A), unstrained region (B), and a region of inhomogeneous strain which also includes crack tip (C).

Measurements of Tear Strength

All measurements were carried out on trouser-leg test specimens as shown in Figure 1, using an Instron tensile tester. The test specimen in the form of tapes of about 2.2–2.5 mm wide, 0.05–0.08 mm thick, and 100 mm long were cut from uniaxially oriented continuous tapes. An initial cut of about 20 mm length was inserted along the center line of the specimen by means of a razor blade whose edge was held perpendicular to the plane of the tape and inserted from the end, i.e., in the direction in which the crack was to be propagated, thus giving a sharp tip to the initial crack. The two free ends thus formed were clamped in the jaws and pulled apart as shown in Figure 1. The value of tearing energy for crack propagation along the orientation direction was calculated from the maximum average steady tearing force (F), recorded at a tear propagation rate of 20 mm/min and at room temperature, using eq. (2):

$$G_c = 2F/t \tag{2}$$

where t is the thickness of tape. The contribution of the energy spent in drawing and bending of free ends of the tear test specimen to the tear energy for films of various thickness have been reported by Gent and Jeong[20] and is relatively small for oriented thin films. This may increase to about 15–20% of the total tearing energy in case of less oriented materials because of the relatively large tearing force involved in tearing of such materials. For determination of tear energy, the maximum average tear force was taken as F, because it is argued that this force must be attained to allow tearing to proceed either by pulling or breaking the crossover fibrillar network in the vicinity of the crack tip and that the subsequent reduction in force is due to the relaxation of legs as the tear advances.[20]

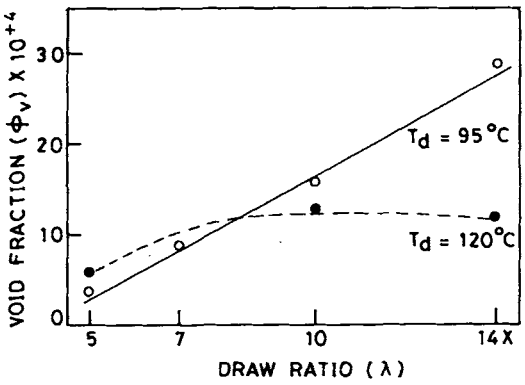

Figure 2 Volume fraction of voids as a function of draw ratio for HDPE tapes.

Optical Microscopy

Fracture surface near the advancing crack tip of large number of oriented tapes was observed by optical microscope. For this purpose the crack tip and the surrounding material containing fracture surface were cut from the test specimen and mounted on microslides. These specimens were then viewed under a projectina optical microscope equipped with photographic system to study the fracture surface and for recording the optical micrograph.

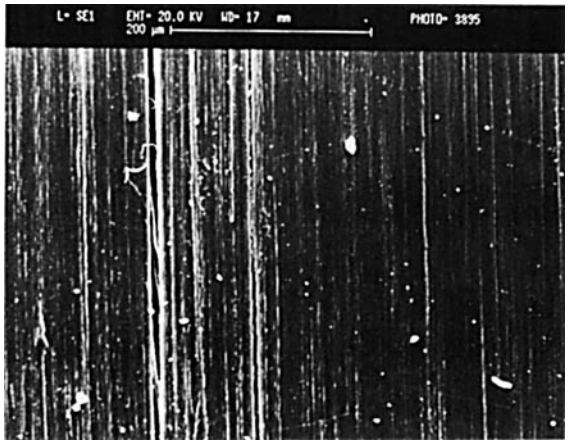

Figure 3 Micrograph of the surface of HDPE tape showing axial crack formation (draw ratio 14×, drawing temperature 95°C).

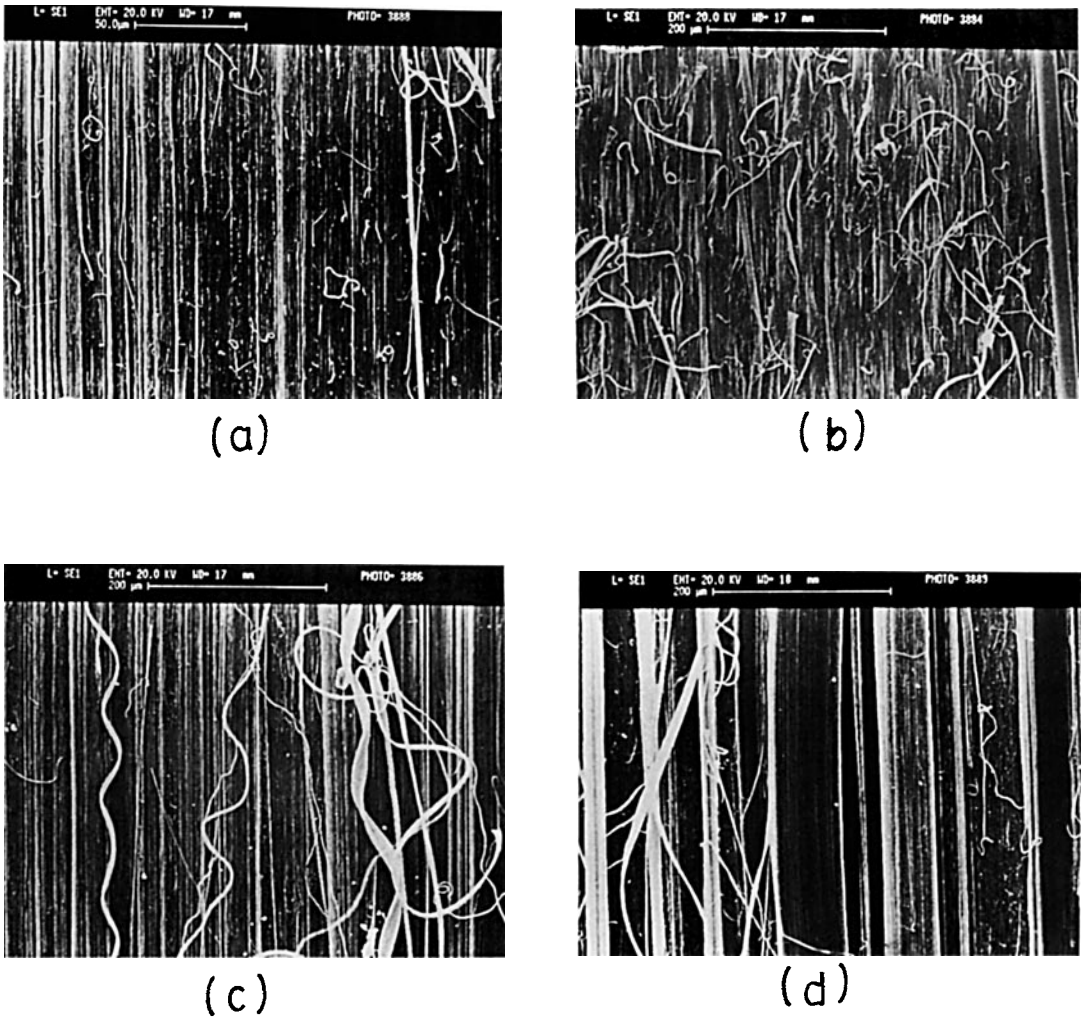

Figure 4 Micrographs of the interior fibrillar structure of peeled HDPE and blended tapes (draw ratio 10×, drawing temperature 95°C). (a) HDPE (control); (b) 10 EVA; (c) 9 EP_bC 3.5; (d) 50 EP_bC 3.5.

Scanning Electron Microscopy

The fracture surface of selected specimens were observed under scanning electron microscope (SEM) for finer details. A Cambridge stereoscan S-360 SEM was used for this purpose. The surface of several specimens were peeled to expose the interior fibrillar structure and viewed under SEM. The micrographs of the crack tip and the surrounding region of trouser-leg test specimens were also obtained.

RESULTS AND DISCUSSION

Fibrillar Structure of Drawn Tapes

The dependence of volume fraction of voids (ϕ_v) of HDPE tapes on draw ratio and drawing temperature is shown in Figure 2. It is seen that, volume fraction of voids increases with draw ratio, particularly when drawn at 95°C. This effect is attributed to the transformation of inhomogeneities and defects created during initial stages of drawing (necking) into microvoids elongated along the drawing direction as a consequence of interfibrillar slippage during deformation of fibrous structure.[20–23] With further increase in draw ratio these microvoids may become more elongated and may coalesce, and cracks having cross-sections larger by an order of magnitude would be formed. These cracks cause fibrillation of drawn tapes. An SEM micrograph of the HDPE drawn tape (Fig. 3) illustrates this phenomenon. The decreased volume fraction of voids for a drawing temperature of 120°C is associated with the greater perfection in packing of fibrillar elements.

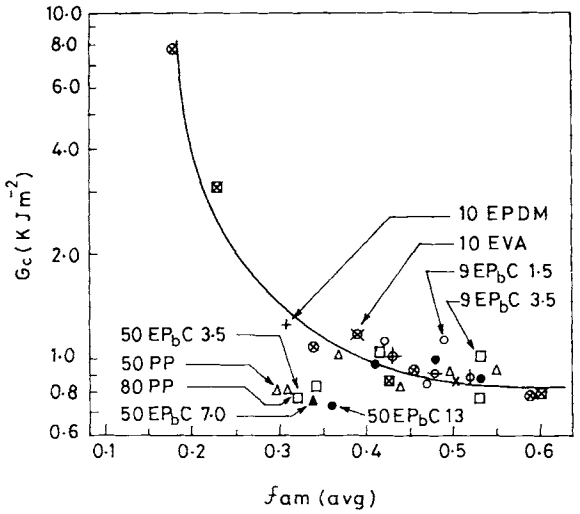

Figure 5 Fracture surface energy vs. amorphous phase orientation for HDPE and blended tapes. (×) HDPE (control); (⊗) HDPE (draw ratios 3×, 5×, 7×, 14×; T_d = 95°C); (⊠) HDPE (draw ratios 3×, 5×, 7×, 14×; T_d = 120°C); (Φ) 10 HMWPE; (⊖) 10 LLDPE; (⊕) 10 LDPE; (⊗) 10 EVA; (+) 10 EPDM; (△) HDPE/PP; (○) HDPE/EP$_b$C 1.5; (□) HDPE/EP$_b$C 3.5; (▲) HDPE/EP$_b$C 7.0; (●) HDPE/EP$_b$C 13. For details, refer to Tables III and IV.

The results on various void parameters of drawn blended tapes are summarized in Table III. In case of HDPE blended tapes drawn to 10× at 95°C, the void dimensions parallel to the tape axis increased from 144 Å for HDPE tape to 156 Å for 10 EVA blend; the dimensions perpendicular to the tape axis increased from 122 to 151 Å for HDPE tape and EVA blend, respectively. For HDPE/PP and HDPE/EP$_b$C blends there appear to be even large voids compared with HDPE/ethylene copolymer

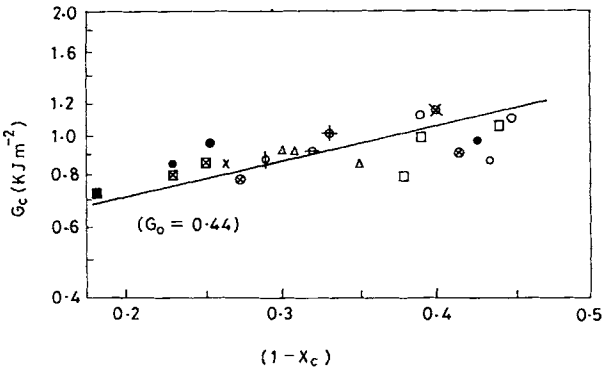

Figure 6 Fracture surface energy vs. fraction of amorphous phase for HDPE and blended tapes. Symbols as indicated in Fig. 5. Solid square represents HDPE sample of draw ratio 14×, drawing temperature 95°C, heat-set at constant length for 40 min at 125°C.

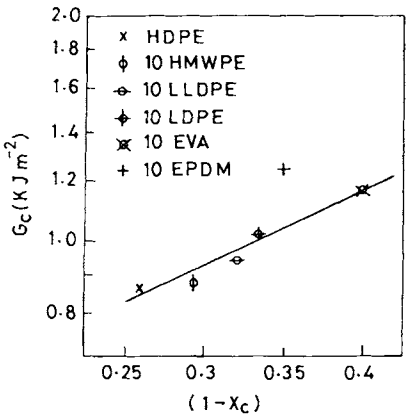

Figure 7 Fracture surface energy vs. fraction of amorphous phase for HDPE (control) and HDPE/ethylene copolymer blends. Symbols as indicated in Fig. 5.

blends. For these blends the typical void dimensions are in the range of 159–191 and 148–174 Å in the meridional and equatorial directions, respectively. An examination of the SEMs shown in Figure 4 clearly support these results. The micrographs of 10 EVA specimens shown in Figure 4(b) indicate little evidence of any fibrillation or presence of axial cracks, and the fibrillar structure is more or less homogeneous. On the other hand, fibrillar morphology of HDPE/EP$_b$C blends of similar blend composition shown in Figure 4(c) indicates a coarse and open fibrillar structure with large interfibrillar cracks oriented parallel to the draw direction.

In light of the results it also appears that voids in 50 PP and 50 EP$_b$C blends are comparatively bigger and the fibrillar elements of these blends show wide variation with respect to lateral size and its orientation compared with other blend specimens [Fig. 4(d)]. This is in accordance with the reported immiscibility of PE and PP blend components at

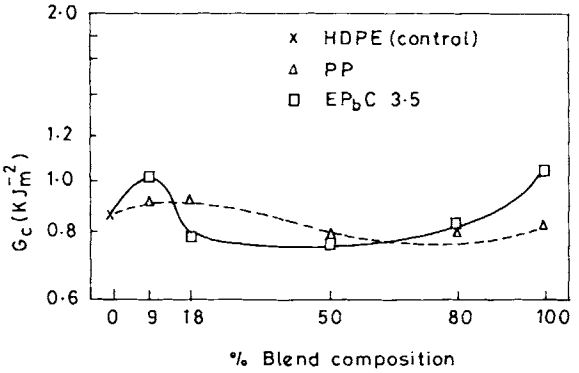

Figure 8 Fracture surface energy vs. blend composition for HDPE/PP and HDPE/EP$_b$C 3.5 blends.

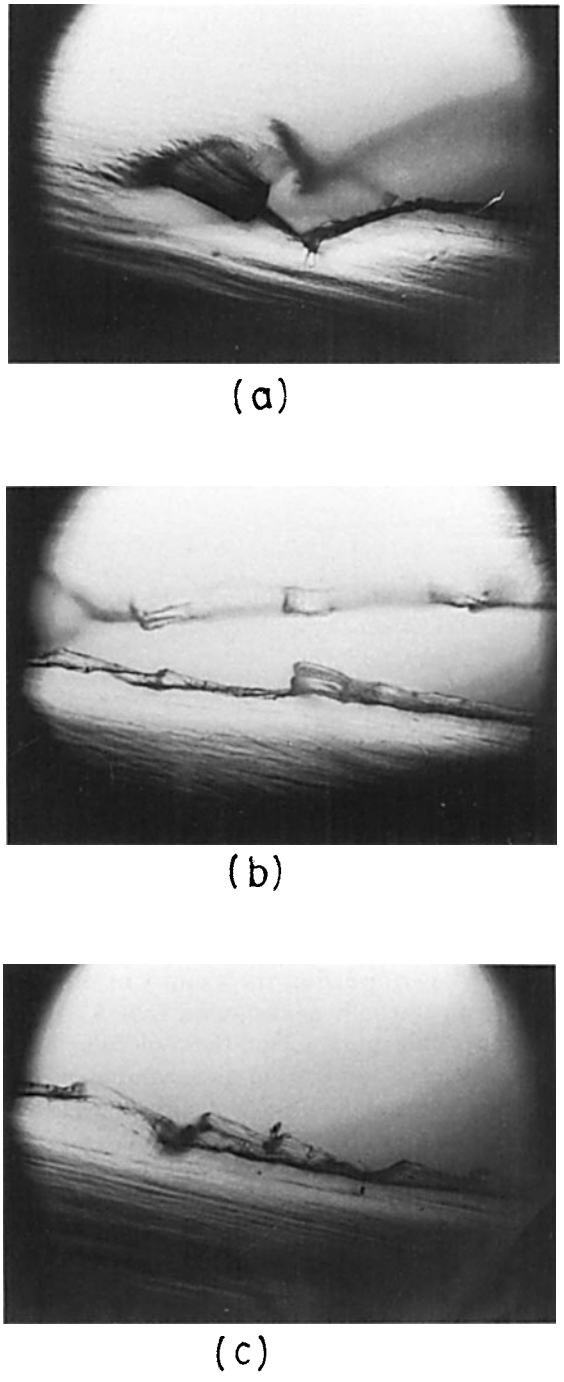

Figure 9 Micrographs of (a) crack tip; (b) and (c) fracture surface of HDPE tape (draw ratio 5×, drawing temperature 95°C).

50% blend composition.[13,25-27] It is suggested that poor interfacial adhesion prematurely initiates the interfacial slippage during drawing, in which damage may occur to one of the phases of blend if the draw ratio applied exceeds the limit for one of the blend components, resulting in elongated voids and axial cracks in the drawing direction.[28-31]

The relatively smaller voids and lower volume fraction of voids observed for HDPE/ethylene copolymer blends of 10% blend composition are related to partial miscibility of blend components[32-35] and homogeneous deformation of fibrous structure in the post-neck deformation region.[12,13] This makes the fibrillar structure more compact and less susceptible to voiding and results in axial crack formation parallel to the drawing axis.

Effect of Amorphous Phase Orientation on G_c

Figure 5 shows the relationship between fracture surface energy and amorphous phase orientation of drawn HDPE and blended tapes. The slope of G_c vs. f_{am} curve is steep at the beginning where G_c drops rapidly from 8.0 kJ m^{-2} to about 1.0 kJ m^{-2} as the f_{am} increases from approximately 0.2 to 0.4. Beyond this region there is a steady decrease in G_c with f_{am} that is followed by a final leveling off at still higher

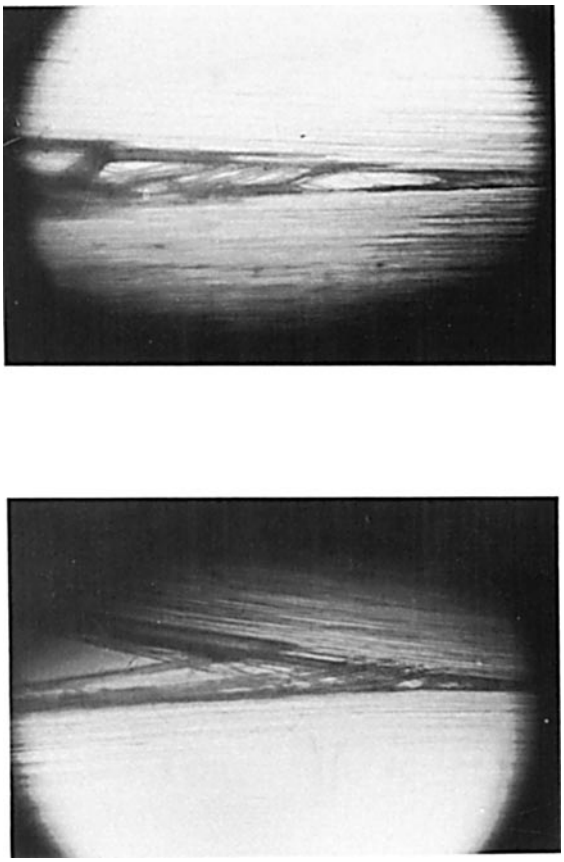

Figure 10 Typical micrographs of crack tip showing fibrillar network in the vicinity of crack tip (draw ratio 10×, drawing temperature 95°C).

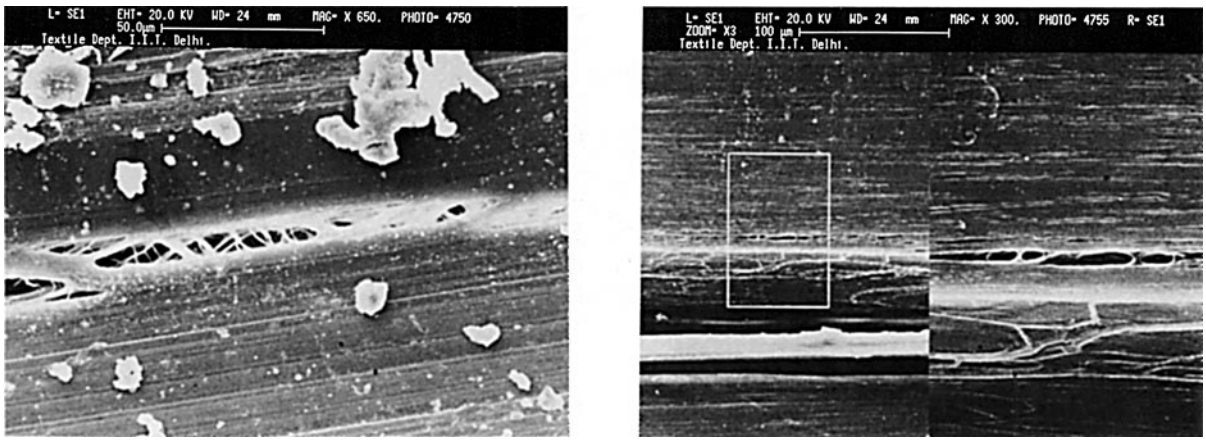

Figure 11 Typical micrographs of the fracture surface showing pulled out fibrillar elements (draw ratio 10×, drawing temperature 95°C).

f_{am} values. From intermediately oriented HDPE tapes ($\lambda = 3\times$; $f_{am} = 0.18$) to relatively more oriented HDPE tapes ($\lambda = 7\times$; $f_{am} = 0.41$), the value of G_c falls by a factor of about 10. A further increase in amorphous phase orientation, i.e., beyond 0.4, has very little effect on G_c, and the values of G_c vary between 1.0 and 0.8 kJ m^{-2}.

The observed dependence of G_c on f_{am} can tentatively be ascribed to the structural and morphological changes occurring during plastic deformation and orientation process. The significant reduction in tear energy of drawn tapes in the initial stages of deformation, i.e., between f_{am} of 0.2 and 0.4 is related to the gradual transformation of lamellar structure of undrawn tapes to a highly oriented fibrillar structure and the associated decrease in the amount of plastic work performed in the vicinity of the propagating tear crack. It is suggested that for drawn tapes of fibrillar morphology, the molecular orientation parallel to the tearing direction has already caused the plastic deformation and alignment of molecular chains and hence has pre-empted the plastic flow process. As a result of this, a considerable part of crack resistance may consist of the energy

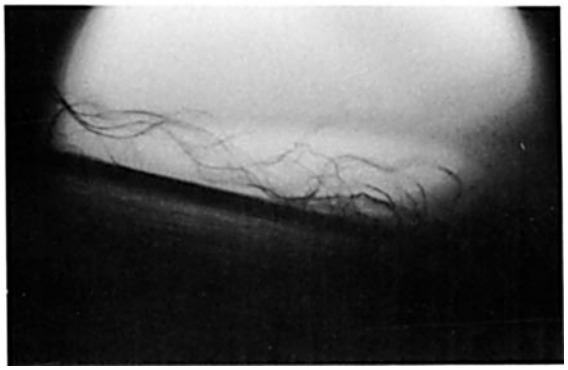

Figure 12 Typical micrographs of the crack tip showing secondary cracks and voids preceding crack tip (draw ratio 10×, drawing temperature 95°C).

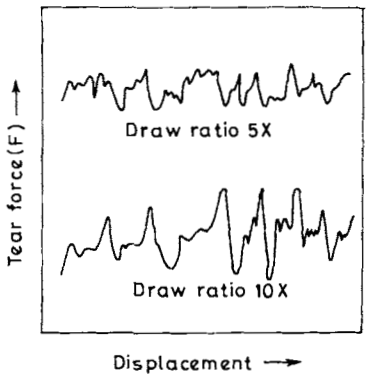

Figure 13 Typical tearing force vs. displacement curves for HDPE tapes of draw ratios 5× and 10×.

expended during the growth and propagation processes. In this case, the crack resistance may be defined as the deformation energy per unit area of advancing crack plane spent in a specific volume around the advancing crack.

Second, as we have shown earlier, the structural transformation is accompanied by the formation of a large number of voids and microcracks running parallel to the axial direction. This, in turn, decreases the interfibrillar cohesion and causes rapid growth and propagation of tear crack as these structural defects act as stress concentrators and prevent the viscous flow of material in the vicinity of propagating crack tip. The increase of amorphous phase orientation beyond 0.4, however, has a little effect on gross fibrillar structure and morphology of drawn tapes. This is reflected in the corresponding values of G_c.

Effect of Fraction of Amorphous Phase on G_c

In this section an attempt has been made to correlate the fracture surface energy with the fraction of amorphous phase $(1 - X_c)$, and the results are presented in Figure 6. For this purpose specimens having fully developed fibrillar morphology ($f_{am} > 0.4$) were selected. Separation of these specimens was necessary to ensure comparable structural and morphological features. From the figure, it is seen that fracture surface energy of drawn tapes steadily increases with an increase in the fraction of amorphous phase. The increase of G_c with $(1 - X_c)$ at nearly comparable f_{am} appears to arise from plastic yielding and molecular flow at the tear tip, which takes place to an increasing extent with increase in $(1 - X_c)$. It is suggested that the development of a homogeneous stress field of sufficient magnitude to induce co-operative plastic yielding and molecular flow around the crack tip of fully drawn tapes depends directly on the fraction of amorphous phase.

To obtain information about the "intrinsic tear strength" or "threshold fracture energy" (G_0), independent of plastic yielding and dissipation processes, an extrapolation of G_c vs. $(1 - X_c)$ curve was made to zero fraction of amorphous phase. The value of G_0 obtained by this procedure is about 0.44 kJ m^{-2}. This value is smaller than those reported by Chiu et al.[8] and Gent and Jeong.[9] However, it is still relatively large in comparison with the theoretical and experimental estimates of G_0 for hydrocarbon elastomers, i.e., from 0.02 to 0.1 kJ m^{-2}.[36-38] This discrepancy may be attributed to the local adiabatic heating effects and the associated molecular flow in the vicinity of the growing crack.

Effect of Blending Various Ethylene Copolymers to HDPE on G_c of Blended Tapes

Figure 7 shows the relationship between G_c and $(1 - X_c)$ for various HDPE/ethylene copolymer blends. It is seen that the enhanced fracture surface energy of drawn blended tapes is associated with the increased fraction of amorphous phase. The G_c of HDPE control specimen is lowest while the 10 EPDM blend is highest. Very similar results are also observed for $(1 - X_c)$, where the amorphous content shows an increase from 0.26 for HDPE control specimen to about 0.4 for 10 EVA and 0.35 for 10 EPDM blends.

The increase in amorphous phase fraction of HDPE blends with addition of a small amount of ethylene copolymers is a consequence of altered crystallization mechanism of HDPE component in the presence of poorly crystallizable ethylene copolymer molecules. In two recent papers,[12,13] the authors studied the crystallization behavior and structural features of HDPE/ethylene copolymer blends. It was found that these blends are partially miscible in nature, which depending on the co-unit concentration of ethylene copolymers leads to (i) a decrease in overall crystallinity of blends, (ii) formation of a denser molecular network, and (iii) enhanced interfibrillar cohesion due to a higher degree of interfibrillar connections. The increase in G_c of HDPE by adding small amount of ethylene copolymers is, therefore, related to the increased fraction of amorphous phase, enhanced interfibrillar adhesion, and denser molecular network. These morphological changes help in the initiation of homogeneous plastic flow of amorphous phase around the propagating crack tip by creating a large number of secondary microcracks and deformation zones. This proposition is supported by the findings of Clements et al.,[5] who reported improvement in G_c for oriented sheets of high-molecular-weight polyethylene and ethylene copolymer.

Effect of Blend Composition on G_c of HDPE/PP and HDPE/EP_bC Blends

Figure 8 shows the relationship between fracture surface energy and blend composition for HDPE/PP and HDPE/EP_bC 3.5 blends. The major feature of these plots is a markedly larger value of G_c for 9EP_bC 3.5 blend. This is in accordance with our earlier results on tensile properties of these blends[13] and is associated with the development of interconnected molecular network, a large reduction in degree of crystallinity, and smaller crystals. The in-

crease in blend composition beyond 9% shows a gradual decrease in G_c for both HDPE/PP and HDPE/EP_bC 3.5 blend systems, and the G_c vs. blend composition curves approach their lowest values around 50% blend composition. The observed phenomenon is considered to be due to gradual increase in phase segregation of blend components, an increase in volume fraction of voids, formation of wider and more elongated voids, and the development of axial cracks. The SAXS results on voids (Table III) and SEM micrographs (Fig. 4) of these blends clearly support this proposition.

The most noticeable result at higher blend composition range, however, is the significantly higher value of G_c for 100 EP_bC 3.5 specimen. This value of G_c is about 25 and 22% higher than PP and HDPE homopolymer tapes, respectively. This is in agreement with the increased fraction of amorphous phase. The another possible cause of improved G_c may relate to the molecular network. In a block copolymer of ethylene and propylene, the mechanical connections between fibrils and the molecular network as a whole are presumably more highly developed because of altered crystallization behavior of PP segments of EP_bC copolymer molecules.

Fracture Behavior and Fracture Surface Morphology of Drawn Tapes

Figures 9–12 show typical crack tips and fracture surfaces observed for various specimens that had reached stable tearing. It is seen from the micrographs of Figure 9 that the largest G_c for HDPE tapes at draw ratio 5× is associated with ductility. The trough at regular intervals caved in on the fracture surfaces, and the absence of any fibrillar elements protruding on the surfaces clearly indicates that tearing of the tapes in this case is indeed associated with extensive plastic yielding in the vicinity of the crack tip.

The typical nature of crack tip and fracture surface morphology of oriented fibrillar tapes having low G_c values is shown in Figures 10–12. The torn surfaces of these specimens show a fibrillar nature with a dense network of fibrillar elements near the crack tip bridging two legs of the specimen. The crack tip diameter of these tapes is also less clearly defined than a low-oriented specimen, i.e., HDPE tapes of 5× and 7× draw ratios, and is notably much smaller. This effect is related to the complete transformation of lamellar to oriented fibrillar structure and the associated decrease in viscous flow of amorphous phase in the vicinity of the propagating crack tip.

In most of the cases it was also evident that void formation preceded the propagating crack tip. The SEM micrographs of Figure 12 show a typical void ahead of the crack tip in oriented fibrillar specimens. Two or three fibrillar elements are observed to bridge the longitudinal void. Fibril crossovers with multiple microcracks are also evident near the crack tip. Such fracture surface morphology presumably is a result of the presence of elongated voids at weaker interfibrillar regions, poor interfibrillar adhesion, and strained but unruptured fibrillar elements linking the two neighboring fibrils. This leads to void growth in a noncolinear fashion, i.e., microcracks forming on either side of the major crack axis. As the major crack propagates, these microcracks become incorporated into the growing crack and fibrils bridging the microcracks, and a major crack now cross the major crack and give rise to the observed network structure of fibrillar elements near the crack tip (see Fig. 10). On further propagation of the crack, these fibrillar elements get strain hardened and eventually pulled out of the matrix, which gives the characteristic irregularity of fracture surfaces. This effect is also reflected in tear force-displacement curves as indicated by oscillation of tear force about a constant mean value to a larger extent. This is shown in Figure 13, along with the characteristic tear force–displacement curve of HDPE tape of 5× draw ratio.

CONCLUSIONS

The fracture surface energy of drawn tapes in orientation direction is of the order of 1 kJ m^{-2}. The fracture surface energy of drawn tapes depends on the volume of material that yield before tear propagates. The work of plastic deformation is then included in G_c. In consequence, the tear energy of drawn tapes increases with increasing fraction of amorphous phase. The effect of increasing amorphous phase orientation on G_c is rather complex. The G_c of drawn tapes fell by a factor of about 10 as the amorphous phase orientation was increased from 0.2 to 0.4. At higher orientation level, i.e., beyond $f_{am} = 0.4$, no significant change in value of G_c is observed. The latter samples however show an increase in G_c with fraction of amorphous phase.

The best prospects for production of oriented polyethylene tapes with reasonably good resistance to tearing are obtained by blending about 10% of EVA, EPDM, and EP_bC copolymers to high-density linear polyethylene.

REFERENCES

1. R. J. Samuels, *Polym. Eng. Sci.*, **25,** 875 (1985).
2. G. E. Anderton and L. R. G. Treloar, *J. Mater. Sci.*, **6,** 562 (1971).
3. G. L. A. Sims, *J. Mater. Sci.*, **10,** 647 (1975).
4. R. A. Rivlin and A. G. Thomas, *J. Polym. Sci.*, **10,** 291 (1953).
5. J. Clements and I. M. Ward, *J. Mater. Sci.*, **18,** 2484 (1983).
6. E. H. Andrews, *Fracture in Polymers,* American Elsevier, New York, 1961.
7. J. P. Berry, *J. Appl. Polym. Sci.*, **33,** 1741 (1962).
8. D. S. Chiu, A. N. Gent, and J. R. White, *J. Mater. Sci.*, **19,** 2622 (1984).
9. A. N. Gent and J. Jeong, *J. Mater. Sci.*, **21,** 355 (1986).
10. N. Roy Choudhury and A. K. Bhoumik, *J. Mater. Sci.*, **25,** 161 (1990).
11. L. A. Polovikhina, I. G. Shimko, and M. P. Zverev, *Fibre Chem.*, **10,** 13 (1978); *Khimicheskie Volokna,* **1,** 12 (1978).
12. S. J. Mahajan, B. L. Deopura, and Yimin Wang, *J. Appl. Polym. Sci.*, **00,** 0000 (1996).
13. S. J. Mahajan, B. L. Deopura, and Yimin Wang, *J. Appl. Polym. Sci.*, **00,** 0000 (1996).
14. A. Guinier, *X-Ray Diffraction,* Freeman, San Francisco, 1963.
15. A. Guinier and G. Fournet, *Small-Angle X-Ray Scattering,* Wiley, New York, 1955, p. 70, 187.
16. F. J. Balta-Calleja and C. G. Vonk, *X-Ray Scattering of Synthetic Polymers,* Elsevier, Amsterdam, 1989, p. 241.
17. Y. Sasanuma, Y. Kitano, and A. Ishitani, *J. Mater. Sci.*, **24,** 1133 (1989).
18. R. P. Runt, in *Encyclopedia of Polymer Science and Engineering,* Vol. 4, 2nd Ed., H. F. Mark, N. M. Bikales, C. G. Overberger and G. Menges, Eds., Wiley-Interscience, New York, 1986, p. 482.
19. H. Bodaghi, J. E. Spruiell, and J. L. White, *Int. Polym. Process.*, **III**(2), 100 (1988).
20. A. N. Gent and J. Jeong, *Intern. J. Fracture,* **29,** 157 (1985).
21. D. C. Prevorsek, Y. D. Kwon, and R. K. Sharma, *J. Mater. Sci.*, **12,** 2310 (1977).
22. A. Peterlin, in *Ultra-High Modulus Polymers,* A. Ciferri and I. M. Ward, Eds., Applied Science Publishers, London, 1977, p. 279.
23. Ch. Oudet and A. R. Bunsell, *J. Mater. Sci.*, **22,** 4292 (1987).
24. A. Peterlin, *Int. J. Fracture,* **11,** 761 (1975).
25. P. Robson, G. J. Sandilands, and J. R. White, *J. Appl. Polym. Sci.*, **26,** 3515 (1981).
26. S. Danesi, in *Polymer Blends: Processing, Morphology and Properties,* Vol. 2, M. Kryszewski, A. Galeski and E. Martuscelli, Eds., Plenum Press, New York, 1979, p. 35.
27. G. A. Gallagher, R. Jakeways, and I. M. Ward, *J. Appl. Polym. Sci.*, **43,** 1399 (1991).
28. T. Kitao, H. Kobayashi, S. Ikegami, and S. Ohya, *J. Polym. Sci., Polym. Chem. Ed.*, **11,** 2633 (1973).
29. F. Coppola, R. Greco, E. Martuscelli, H. W. Kammer, and C. Kummerlowe, *Polymer,* **28,** 47 (1987).
30. A. J. Lovinger and M. L. Williams, *J. Appl. Polym. Sci.*, **25,** 1703 (1980).
31. D. R. Paul, in *Polymer Blends,* Vol. 2, D. R. Paul and S. Newman, Eds., Academic Press, New York, 1978, p. 189.
32. S. R. Hu, T. Kyu, and R. S. Stein, *J. Polym. Sci., Polym. Phys. Ed.*, **25,** 71 (1987).
33. R. G. Alamo, R. H. Glaser, and L. Mandelkern, *J. Polym. Sci., Polym. Phys. Ed.*, **26,** 2169 (1988).
34. M. J. Hill, P. J. Barham, A. Keller, and C. C. A. Rosney, *Polymer,* **32,** 1384 (1991).
35. N. K. Kalfoglou, *J. Macromol. Sci. Phys. Ed.*, **B22,** 343 (1983).
36. A. N. Gent and R. H. Tobias, *J. Polym. Sci., Polym. Phys. Ed.*, **20,** 2317 (1982).
37. G. J. Lake and A. G. Thomas, *Proc. Roy. Soc. Lond.*, **A300,** 108 (1967).
38. H. K. Mueller and W. G. Knauss, *Trans. Soc. Rheol.*, **15,** 217 (1971).

Received June 16, 1994
Accepted October 7, 1995